Macromolecules
Cite This: Macromolecules 2019, 52, 7638−7645
Article
pubs.acs.org/Macromolecules

Morphologies of Polyisoprene-Grafted Silica Nanoparticles in Model Elastomers

Marine Bonnevide,[†,‡,§] Andrew M. Jimenez,[∥] Deboleena Dhara,[∥] Trang N.T. Phan,[‡] Nicolas Malicki,[§] Zaid M. Abbas,[⊥,#] Brian Benicewicz,[⊥] Sanat K. Kumar,*[,∥] Marc Couty,[§] Didier Gigmes,[‡] and Jacques Jestin*[,†]

[†]Laboratoire Léon Brillouin, UMR 12, Université Paris-Saclay, IRAMIS/CEA Saclay, 91191 Gif-sur-Yvette Cedex, France
[‡]Aix Marseille Univ, CNRS, Institut de Chimie Radicalaire, UMR 7273-Campus Scientifique St Jérôme, Service 542, 13397 Marseille Cedex 20, France Marseille, France
[§]Manufacture Française des Pneumatiques MICHELIN, Site de Ladoux, 23 Place des Carmes Déchaux, F-63 040 Clermont-Ferrand Cedex 9, France
[∥]Department of Chemical Engineering, Columbia University, New York, New York 10027, United States
[⊥]Department of Chemistry and Biochemistry, University of South Carolina, Columbia, South Carolina 29208, United States
[#]Department of Chemistry, Wasit University, Hay Al-Rabea, Kut, Wasit 52001, Iraq

Supporting Information

ABSTRACT: We control nanoparticle (NP) dispersion by leveraging the entropic and enthalpic effects associated with mixing silica NPs grafted with polyisoprene (PI) chains into matrices of varying degrees of chemical dissimilarity. Previous work in this area has primarily focused on entropic factors alone, and hence, this work represents a significant advance over the current state-of-the-art. We show using a combination of transmission electron microscopy/small-angle X-ray scattering that mixing grafted particles with PI matrices of identical microstructure yields dispersion states as found in the literature for such entropic systems. However, replacing the PI matrix chains with dissimilar matrices leads to an introduction of enthalpic interactions that, in some cases, can drastically change the resulting morphology. In particular, while slightly different PI microstructures for the grafted and free chains only yield moderated differences, using styrene−butadiene copolymers as a matrix leads to a completely different behavior. In the last case, phase separation becomes more likely with the increasing graft length, while the PI system (whose behavior is dominated by entropic factors) shows the opposite behavior. Tuning the relative importance of enthalpic versus entropic factors is thus another tool in controlling the self-assembled structure of NPs, which gives rise to enhanced macroscopic properties in the composite.

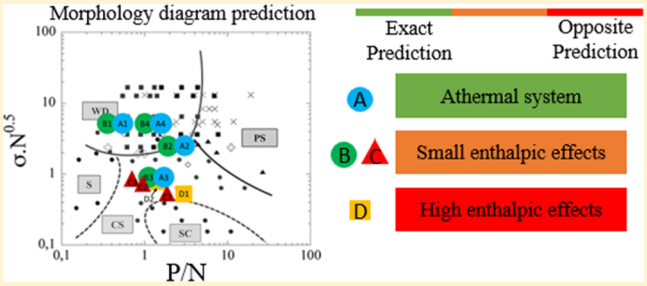

1. INTRODUCTION AND BACKGROUND

The addition of inorganic nanoparticles (NPs) to polymer matrices is a widely used strategy to improve the electrical,[1] optical,[2] mechanical,[3] flame retardancy,[4] or gas barrier[5] properties. This improvement of properties is related to the specific contact area between fillers and matrix which increases as the particles size decreases (at fixed loading), so long as the particles maintain the same state of dispersion.[6−9] Generally, adding ∼5% wt of 10 nm filler allows one to obtain the same mechanical property enhancement as with 30% wt of micron-sized particles.[10] However, NPs tend to aggregate, that is, the dispersion gets progressively worse with the decreasing NP size, resulting in a reduction of the specific contact area with the matrix[11] with deleterious effects on final properties.[12] Over the last few years, significant efforts have been made to develop new strategies for controlling the NP dispersion, in particular by grafting the NP with polymer chains with the same chemistry as the matrix; variations of the grafting densities and the ratio of the lengths of the grafted (N) and free (P) chains allows one to access a range of NP dispersion states.[13,14] Kumar et al. used a compilation of experiments and numerical simulations on conventional polymers (polystyrene PS, poly(methyl methacrylate) (PMMA), where the grafts continue to have the same chemical structure as the matrix), to delineate regions in parameter space where individual NP dispersion, phase separation, small clusters, and connected sheets form.[15] While these results are interesting, it is critical to examine if these findings have relevance to commercially

Received: July 16, 2019
Revised: September 16, 2019
Published: October 2, 2019

Downloaded via UNIV OF SOUTH CAROLINA COLUMBIA on January 15, 2020 at 19:36:16 (UTC).
See https://pubs.acs.org/sharingguidelines for options on how to legitimately share published articles.

© 2019 American Chemical Society

DOI: 10.1021/acs.macromol.9b01479
Macromolecules 2019, 52, 7638−7645

Table 1. PI Microstructure

	M_w (kDa)	$Đ$ (dispersity)	% 1,4 trans	% 1,4 cis	% 1,2	% 3,4
PI-RAFT-SiO_2	28−120	1.4−2.1	75	20	1.3	3.7
PI-NMP-SiO_2	20−45		43.7	24.6	13.2	18.6
PI-RAFT	52	1.8	75	20	1.3	3.7
PI-Sigma	35	3.5−4	24.8	75.2		

elastomeric systems, where the grafts and matrices may not always have the same chemical (micro) structure.[16,17] Among the various elastomers, polyisoprene (PI) and its copolymers are of great interest and are used for medical applications,[18,19] in sporting goods,[20] and in the automotive industry[21−23] due to their excellent break, wear, and tear strengths.

It is important to stress that NP agglomeration can be even more important in these practically important situations because of the very poor energetic interactions between typical NPs and elastomers.[24] Previously, several solutions have been proposed to improve the dispersion of NPs in elastomers. Bouty et al.[25,26] studied the dispersion of silica NPs with an average radius of 8 nm in Styrene−Butadiene-Rubber (SBR) by modifying the surface with (i) a coupling agent (bis-(triethoxysilyl)propyl tetrasulfide) which can covalently bond with the matrix chains via the sulfur bond or (ii) a coating agent (octyltriethoxysilane) which is known to improve the enthalpic compatibility with the polymer. They demonstrated that the coupling agent leads to smaller aggregates as compared to the coating agent which yields larger and ramified objects, though neither approach allowed them to obtain individual NP dispersion. A similar approach was also investigated by Baeza et al.[27] using functionalized SBR chains, and in situ grafting the SBR chains to the NPs. Such approaches are strongly limited by the reaction of the chains to the NP surfaces. To circumvent this limitation, one can use controlled polymer grafting of the particle (as previously described for conventional polymers) before the NPs are dispersed in the matrix. Hosseini et al.[28] compared the effects of modifying precipitated amorphous silica (specific surface area of 180 m^2/g) with a coupling agent or with hydroxyl-terminated polybutadiene (HTPB) of 2800 $g\cdot mol^{-1}$. They showed that the dispersion of silica in a SBR matrix was more uniform and homogeneous when it was modified with HTPB, but this grafting also led to a worsening of mechanical properties, presumably due to a disruption of the filler network and the lack of strong filler polymer bonding. These results however assert that it is necessary to optimize and control grafting parameters such as grafting density and chain length to obtain the optimal dispersion state for improved mechanical properties. To our knowledge, the only example of surface polymerization of isoprene on to silica NPs using a reversible-deactivation radical polymerization technique was recently reported by Khani et al.[29] They first synthesized chain-transfer agent-functionalized silica NPs and then polymerized isoprene onto the surfaces using reversible addition fragmentation chain transfer (RAFT). They also studied the dispersion of PI-grafted SiO_2 NPs in a PI matrix using transmission electron microscopy (TEM) and showed compatibility between the grafted NPs and the matrix. In the current work, we present the compatibility of PI-grafted SiO_2 synthesized from both surface initiated (SI)-RAFT as well as nitroxide mediated polymerization (NMP) in "grafting from" polymerizations of isoprene from silica NPs. The combination of different techniques such as thermogravimetric analysis, small-angle neutron scattering, and size exclusion chromatography allows for a detailed characterization of these polymer-grafted NPs, namely, the resulting grafting density and chain length.[30] Subsequently, we studied their dispersion in elastomeric matrices of different microstructures using small-angle X-ray scattering (SAXS) and TEM showing an evolution of dispersion depending on the grafting density and the ratio of the matrix chain length and the grafted chain length.

2. MATERIAL AND METHODS

2.1. Materials. Spherical SiO_2 NPs (TOL-ST and MEK-ST), with a nominal diameter of 10−15 nm, were provided by Nissan Chemical Company. Ultracel membranes (30, 100 kDa, Merck Millipore), 2-(((dodecylthio)carbonothioyl)thio)propanoic acid (DoPAT) (Strem Chemicals, 97%), tetrahydrofuran (THF) (Carlo Erba Reagents, 99.9%; Fisher, HPLC), pentane (VWR, 95%), *N*,*N*-dimethylacetamide (Aldrich, 99.9%), dicumyl peroxide (Aldrich, 99%), dimethylmethoxy-*n*-octylsilane (Gelest, 95%), 3-aminopropyldimethylethoxysilane (Gelest, 95%), anhydrous methanol (Aldrich, 99.8%), isoprene (Aldrich, 99%), and PI, cis (Aldrich, M_w = 35 000 g/mol) were used as received.

2.2. Sample Preparation. The grafted NPs were synthesized using two techniques to produce PI-grafted silica NPs: SI-RAFT[29] and NMP,[30] designated PI-RAFT-SiO_2 and PI-NMP-SiO_2, respectively. RAFT synthesis was also used to provide free PI chains of the same microstructure as the NP grafted chains, designated PI-RAFT (further details on synthesis are included in the Supporting Information). Additional free polymer chains purchased from Sigma were used as a matrix of dissimilar microstructure, designated PI-Sigma, and Styrene−Butadiene-Rubber SBR (M_w = 54 kDa, 26% styrene; 31% PB 1,2; 23% PB-1,4 trans; 20% PB 1,4 cis, dispersity = 1.1) was provided by Michelin. The microstructures of each can be found in Table 1. The effects from mixing the various microstructures are described in the subsequent results.

Composite samples were solution cast by dissolving free matrix chains at 5 wt % in THF before adding PI-grafted NPs at ∼5 wt % NP core (SiO_2) to the total mass. The resulting mixture was vigorously stirred/vortexed for 2−4 h at room temperature and then probe sonicated before allowing the THF to steadily evaporate off (without boiling), under vacuum, again at room temperature. Our previous work[31] has shown that the NP structures that form, especially in the case of large graft densities, are independent of the particular solvent employed as long as it is favorable to the graft chains. This is likely because the grafts shield the NP core and thus ensure good dispersion in the initial state obtained after solvent casting. In agreement with these notions, we find similar NP structures when toluene or THF is used in sample preparation; on the other hand, xylene (a poor solvent for the grafts) yields agglomerated NPs.

2.3. Scattering and Microscopy Characterization. *2.3.1. SAXS and USAXS.* SAXS experiments were carried out on a Xeuss 2.0 apparatus (Xenocs, France) at the Laboratory Léon Brillouin (LLB NIMBE CEA Saclay). The instrument uses a microfocused Cu Kα source with a wavelength of 1.54 Å and a PILATUS3 detector (Dectris, Switzerland). The experiments were performed with a collimated beam size of 0.3 × 0.25 mm. The sample-to-detector distance was chosen to be 2540 mm to achieve a Q range of 0.004−0.2 $Å^{-1}$. Additional SAXS was performed on a Saxslab Ganesha instrument (Xenocs, France) at the Columbia Soft Matter Laboratory, with the same Cu Kα source and effective Q range. The elastomer films were molded into an aluminum ring and sealed between two Kapton sheets. Scattering from empty beam, Kapton sheets and dark

DOI: 10.1021/acs.macromol.9b01479
Macromolecules 2019, 52, 7638−7645

field were measured independently and subtracted using standard protocols. The data were normalized to absolute units. Modeling and fitting were performed with the SASFIT software. USAXS experiments were carried out on the beamline ID02 at ESRF (Grenoble), with a wavelength of 1 Å (E = 12.4 keV) and two sample-to-detector distances of 1 and 30 m, yielding a total Q range from 2×10^{-4} to 5×10^{-1} Å^{-1}.

2.3.2. Transmission Electronic Microscopy. Samples were cut from the un-cross-linked melt using cryo-ultramicrotomy and imaged using cryo and room temperature TEM. Cryo-ultramicrotomy was performed on a Leica EM FCS microtome at −90 °C with cut speeds varying between 2 and 10 mm/s to obtain sections of thickness ∼100 nm. The sections were collected on a Formvar-coated copper grid and stored in liquid nitrogen prior to imaging on an FEI Talos 120C TEM at 120 kV, equipped with a Gatan OneView camera.

2.3.3. Differential Scanning Calorimetry. Differential scanning calorimetry (DSC) analyses were performed on a TA Instruments (DSC Q20) with the following program (heat−cool−heat cycle): heat from 25 to 50 °C at 10 °C/min, cool to −80 °C at 10 °C/min and heat to 50 °C at 10 °C/min. Heat curves from the second heating are used here.

3. RESULTS AND DISCUSSION

The morphology diagram shown in Figure 1 is a common reference point for helping to determine a priori what kind of

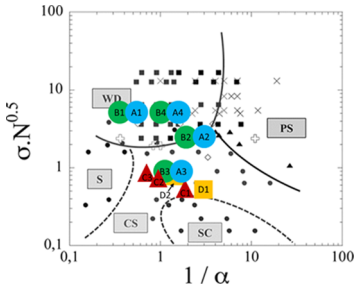

Figure 1. Morphology diagram of polymer-grafted NPs in a polymer matrix, borrowed from Kumar et al.[15] Samples in color represent the various systems studied in this work: (blue circle) PI-RAFT-SiO_2 in PI-RAFT matrix, (green circle) PI-RAFT-SiO_2 in PI-Sigma matrix, (red triangle) PI-NMP-SiO_2 in PI-Sigma matrix, and (yellow square) PI-NMP-SiO_2 in SBR matrix. Data on smaller green circles can be found in the Supporting Information (WD = well dispersed, PS = phase separated, CS = [Connected] Sheets, SC = Small Clusters, S = Strings. Note: $\alpha = N/P$).

NP dispersion one can expect for polymer-grafted NPs in a polymer matrix (σ = graft density, $\alpha = N/P$, where N = degree of polymerization of the grafted chain and P = degree of polymerization of the matrix, see Table 2). This empirical plot is the compilation of data from a variety of polymeric systems but is largely dominated by the athermal system of PS-g-silica in the PS matrix, guided by the theoretical principles from Akcora et al.[31] The N and P values used here are based on the recorded weight average molecular weights, M_w, of the polymers. For highly uniform polymers (low dispersity, $Đ$), the application of this morphology diagram is largely unaffected by the choice of reported molecular weights. However, industrially purchased polymers often report $Đ$ values in the range of 2−4, which could significantly change the expected morphology. For completeness, we include the same plot in the Supporting Information using instead the number average molecular weight, M_n. While some papers suggest the use of M_n to more accurately represent the system, we chose to focus here on M_w to capture the influence of the addition of long chains in highly disperse systems. Regardless of molecular weight definition, these systems can experience a transition from dispersed to agglomerated through either decreased wetting of a dense graft with increasing matrix chain lengths (well dispersed—phase separated) or decreasing graft density which exposes the NP core and allows for clustering due to core−core attractions (well dispersed—strings/sheets/small clusters). The latter of course depends on the core-matrix interaction, where a favorably interacting core-matrix system, with smaller van der Waals attractions, can promote good NP dispersion, regardless of NP grafting. The system studied here focuses on silica NPs (hydrophilic cores with relatively low van der Waals attractions, compared to other commonly used NPs) in hydrophobic polymer matrices. Although the morphology diagram appears to encompass these phenomena seamlessly, the root cause for agglomeration is necessary to distinguish, especially when looking at systems with nonzero interaction parameters (χ) between the graft and matrix. Martin et al.[32] show with simulations and experiments that the wetting/dewetting process occurs gradually with changes in χ, whereas agglomeration is a sharper first-order process which occurs with increases in χ. In highly unfavorable mixtures, the grafted NPs can fully phase separate, despite dense polymer grafting, as one would expect to see in immiscible polymer blends like polystyrene and PMMA. The present work attempts to further test the validity of this morphology diagram when enthalpic effects due to mismatched graft and matrix polymers are introduced. Through the use of two separate grafted NPs and three polymer matrices, we produce four unique systems to study: (case A) PI-RAFT-SiO_2 in PI-RAFT—the only system in which the grafted PI is identical in microstructure to that of the matrix and is therefore our athermal starting point, (case B) PI-RAFT-SiO_2 in PI-Sigma—here, the microstructure of the matrix is effectively flipped in the relative ratio of 1,4 cis and trans, (case C) PI-NMP-SiO_2 in PI-Sigma—again the commercial cis PI is used as the matrix but now the grafted chain has a more diverse microstructure, and finally (case D) PI-NMP-SiO_2 in SBR—this system further probes the enthalpic effect by mixing the grafted NPs with a drastically different chemically structured polymer matrix. As is done with many other systems, these are all plotted on the polymer nanocomposite morphology diagram, which uses only the entropic parameters of graft density of chains on the NP surface and the ratio of the degree of polymerization of the grafted and free chains. Figure 1 demonstrates that with all of these systems, we can cover a wide range of the morphology diagram, stretching across more than an order of magnitude on each axis. From this, we could naively expect to find generally well-dispersed and connected sheet morphologies throughout the samples.

Table 2. PI Grafting Parameters

	N (kDa)	σ (chains/nm^2)	P/N ($1/\alpha$)
A1, B1	104	0.15	0.50, 0.34
A2, B2	20	0.15	2.6, 1.8
A3, B3	32	0.035	1.5, 1.1
A4, B4	38	0.25	1.4, 0.90
C1, D1	20	0.03	1.75, 2.88
C2, D2	38	0.03	0.92, 1.49
C3	45	0.03	0.78

3.1. Moving from Athermal to Mismatched Graft/Matrix Microstructures. As a control case, the PI-RAFT-

DOI: 10.1021/acs.macromol.9b01479
Macromolecules 2019, 52, 7638−7645

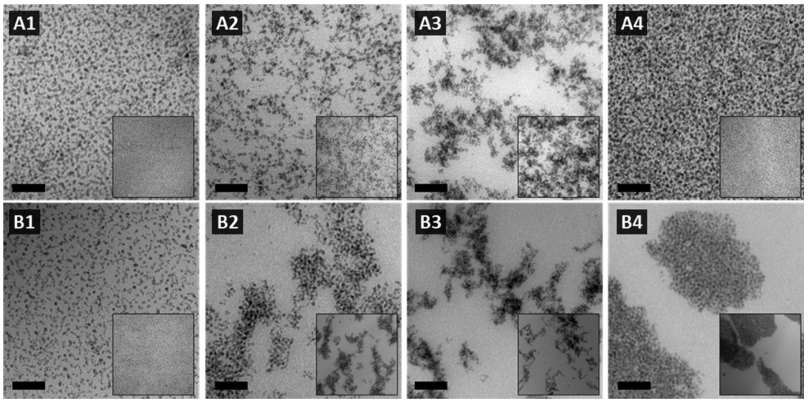

Figure 2. TEM images of PI-RAFT-SiO_2 in (A#) PI-RAFT [matched] matrix and in (B#) PI-Sigma [mismatched] matrix. Samples include (X1) 104 kDa at 0.15 ch/nm^2, (X2) 20 kDa at 0.15 ch/nm^2, (X3) 35 kDa at 0.035 ch/nm^2, and (X4) 38 kDa at 0.25 ch/nm^2. Scale bar is 200 nm for the large images and 1 μm for the insets.

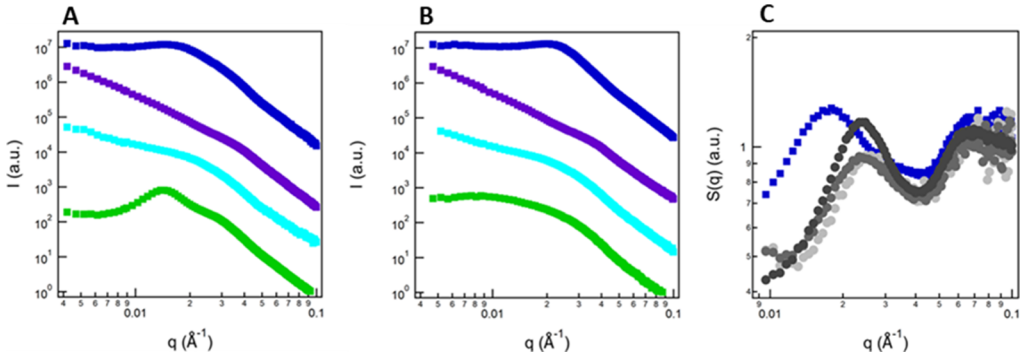

Figure 3. SAXS of PI-RAFT-SiO_2 in (A) PI-RAFT [matched] matrix and in (B) PI-Sigma [mismatched] matrix. Samples include (green) A1/B1, (cyan) A2/B2, (purple) A3/B3, and (blue) A4/B4 with properties noted in Table 2. (C) SAXS structure factors corresponding to the scattering for sample (blue squares) A4 and sample (gray) B4, with increasing NP loadings for darker gray shadings (1, 5, 15 wt %).

SiO_2 NPs were first mixed with PI-RAFT-free polymers of the same microstructure (75% 1,4 trans, samples A1−A4 in Table 2). We focus first on four "A" samples (Table 2), taking us from deep within the well-dispersed region (moderately high graft density, long grafted chains, A1), out to the edge of the phase-separated transition (high graft density, short grafted chains, A4), down slightly toward sheets (moderate graft density, short grafted chains, A2), and finally deep into the sheet-forming region (low graft density, short grafted chains, A3). (Long and short chains are relative to the matrix molecular weights seen in Table 1) Upon TEM analysis, the NP structures appear to correspond very well with what the phase diagram predicts. The two systems sufficiently within the well-dispersed region appear as such (Figure 2A1,A4), whereas the sample down in the sheet region shows high levels of agglomeration (Figure 2A3). The sample on the edge of the boundary, though certainly agglomerating, appears to be somewhere in-between (Figure 2A2). SAXS provides further support for these structural assignments. The well-dispersed systems exhibit structure peaks that can be fit with a Percus−Yevick structure factor. The q^* dependence of the peak on NP loading supports that this change in interparticle spacing is due to NPs that are largely individually dispersed throughout the matrix (Figure 3C). Following the qualitative trends from TEM, the SAXS also shows a relative level of agglomeration between the sheet-forming samples. Deep in the sheet region, the SAXS for A3 shows a low q scattering dependence of $I \sim q^{-2}$, whereas the sample near the phase transition, A2, shows scattering with a scaling exponent of ≈1.5 (Figure 3A). This aligns well with the apparent difference in cluster density seen in TEM (Figure 2).

Building from the structural assignments of the athermal system, the same NPs were then mixed into an industrial PI matrix (75% 1,4 cis) purchased through Sigma, with a notably higher polydispersity. Upon doing so there are immediately obvious changes in only one sample—B4, the one nearest the phase separated region. Unlike the well-dispersed NPs seen throughout the TEM section of the matched matrix sample, the PI-Sigma composite shows large, phase-separated regions of NPs spanning 10 s of micron (Figure 3, B4). Changes in the NP structure for the other composites are less obvious. Moving back to the left on the phase diagram, the NPs with long chains and high graft density still appear to be well dispersed (B1), though a small degree of NP stringing can be seen. As for the sheets, the relative density of agglomerates appears relatively similar for B3, but B2 may have slightly denser NP clusters than its A2 counterpart. Again, SAXS is used to further support these trends. Dividing the scattering intensity by the form factor of the NPs (measured in dilute solution) provides the structure factor, $S(q) = I(q)/P(q)$ (Figure 3C). The composites with sheet-like aggregates (A2/B2 and A3/B3) show strong self-similarity in the NP structure formation, regardless of the matrix (see the Supporting Information). This may be due to changes in the scattering only appearing at q values below the studied range for this system. Both well-dispersed samples appear to have lost some level of their

DOI: 10.1021/acs.macromol.9b01479
Macromolecules 2019, 52, 7638−7645

dispersion but to drastically different degrees. The "B" sample nearest to the phase separated boundary, B4, displays a strong scattering peak around 0.023 Å^{-1}. Using $q = 2\pi/d$, this corresponds to a center-to-center NP spacing of 27 nm, roughly the size of the NP plus grafted shell. This spacing does not change with NP loading, suggesting phase separation (Figure 3C). The sample further from the phase-separated boundary (B1) loses the strong structure peak at the expected well-dispersed NP spacing, seen in the A1 counterpart, but maintains a well-dispersed NP form factor. This suggests that the NPs are still largely dispersed, though to a less uniform degree, that is, the distribution in interparticle spacing has increased (compare Figure 3A,B). The change in dispersion of both initially well-dispersed samples suggests a shrinking of the well-dispersed region for this system. The slight change in interaction of the dissimilar graft-matrix polymers pushed the B4 system toward phase separation through the enthalpically driven dewetting of the grafted brush. This dewetting is likely further assisted by the increase in dispersity of the Sigma matrix, such that the increase in the number of longer chains will promote phase separation. Equally interesting is the more subtle shift in dispersion of A1 to B1. Rather than a sudden phase separation of NPs in this new matrix, we see something more similar to the string morphology, meaning we have managed to shift to different morphologies without changing N nor σ. This minor shift in morphology could suggest the ability to control the sharpness of the dispersion−agglomeration transition by varying the grafted chains, despite having similarly unfavorable interactions with the matrix.

3.2. Moderately Mismatched Microstructure (with NMP Synthesis), Focusing on NP Structures in the Sheet-+Forming Regions. To further study the effect of mismatched microstructure on dispersion, samples synthesized with a different grafting chemistry were mixed again in the industrial PI matrix and studied by SAXS, specifically focusing on the lower region of the phase diagram. The PI polymerized by NMP has a different microstructure than of both the RAFT and Sigma PI, as determined by ^{13}C NMR (Table 1). These samples have a relatively constant graft density of 0.03 chains/nm^2 but with grafted chain with slightly different molecular weights (and polydispersity, Table 2). In Figure 4, we show the variation in scattering intensity of the nanocomposites (the form factor of a primary particle are shown for comparison) when increasing the molecular weight of the grafted chain, keeping all other variables constant. In the high q region, all of the curves more or less superimpose, implying that we are sensitive to the primary particle scattering in this q range. The behavior begins to diverge at low q, where intensity level reflects the formation of clusters composed of primary particles. The morphology of such clusters depends directly on the number of primary particles, namely, the apparent aggregation number (N_{agg}) taken from the extrapolation of the scattered intensity plateau when q tends to zero, as well as the compactness of the clusters, associated with the slope of the power law decrease of the intensity versus q in the intermediate q range (D_f).

We can determine an order of magnitude of the cluster size using the formula $R_{agg} = R_{NP} \cdot N_{agg}^{1/D_f}$, corresponding to a lower bound value of cluster size (i.e., the clusters must be at least this size). The apparent aggregation number and the fractal dimension of the clusters are determined graphically from the structure factors in Figure 4 from the extrapolated plateau at low q and from the slope in the intermediate q range and reported in Table 3.

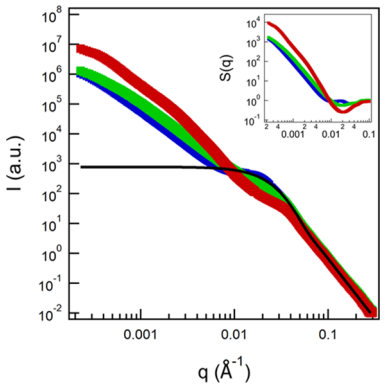

Figure 4. Total scattered intensity for PI-NMP-SiO$_2$ in PI-Sigma with increasing grafted molecular weights corresponding to Table 1: (red) C1, (green) C2, and (blue) C3. The black line is the calculated form factor for a primary NP of mean radius of 6.5 nm with a log-normal distribution of 0.3. (Inset: Corresponding structure factors calculated by dividing the total intensity by the primary NP form factor.)

Table 3. Structure Factor Parameters

sample	N_{agg}	D_f	R_{agg} (nm)	P/N
C1	8850	2.55	212	1.75
C2	1640	2.35	140	0.92
C3	1350	2.26	146	0.78

Evidently, both the apparent aggregation number and the fractal dimension decrease when P/N decreases, meaning that the average size of the clusters is decreasing. The compactness of the clusters is also decreasing, suggesting that they are more ramified. This is further supported with a shift of the particle−particle correlation peak on the structure factor (Figure 4). The peak is initially around 0.04 Å^{-1}, corresponding to two particles in close contact inside the cluster ($d \approx 15$ nm) and moves to around 0.02 Å^{-1} ($d \approx 30$ nm) for sample C3, suggesting that the particles are moving away from each other with the ramification of the cluster structure. We again supplement this characterization of NP dispersion through the use of TEM images (Figure 5). Images are shown at two

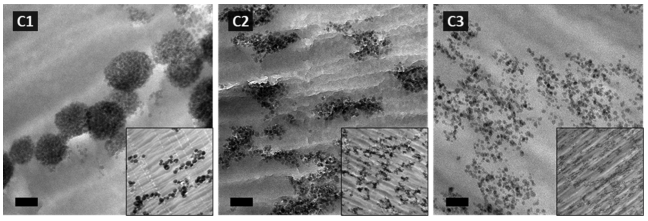

Figure 5. TEM images of PI-NMP-SiO$_2$ dispersed in the PI-Sigma matrix with P/N values (C1) 1.75, (C2) 0.92, and (C3) 0.78. Scale bar is 100 nm for the large images and 1 μm for the insets.

different magnifications to representatively portray the structures forming in system at different scales. The images confirm the formation of clusters of average sizes around 200−400 nm—consistent with the average values determined by SAXS. We can clearly see the decreasing of the compactness of the cluster when decreasing the P/N value which is also consistent with the SAXS analysis. It appears that we have an

DOI: 10.1021/acs.macromol.9b01479
Macromolecules 2019, 52, 7638−7645

obvious transition of particle dispersion with the increasing grafted polymer length. The first two structures (C1, C2) appear to be fairly compact clusters, whereas C3 seems to have a more open structure with a fractal dimension close to 2. This system has provided us with detailed analysis of the transition from small clusters to sheets, right near the expected range in the morphology diagram. The moderated mismatch in polymer microstructure appears to have little effect on this expected transition range.

3.3. Mismatched Chemistry. Taking one last step in understanding the dispersion mechanisms, we now choose to mix the NMP PI-grafted NPs into a SBR matrix. In order to test the compatibility between the grafted chains and the matrix, relative to that of the PI systems, a DSC analysis was performed on mixtures (50 wt %) of PI-NMP and PI-sigma as compared with that of mixtures of PI-NMP and SBR (Figure 6). The T_g of PI-sigma was −60 °C, the T_g of PI-NMP was

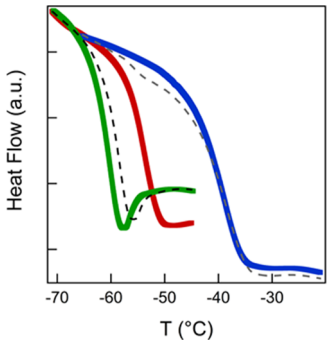

Figure 6. DSC on polymer systems with no NPs showing the glass transitions for (green) PI-Sigma, (red) PI-NMP, (blue) SBR, with the dashed lines corresponding to 50/50 wt % mixtures of (black) PI-Sigma/PI-NMP, and (gray) PI-NMP/SBR.

−53 °C, and we observed only one T_g at −58 °C for the mixture. This confirms for us that the two polymers are indeed miscible. We compare this to the same DSC miscibility test of PI-NMP and SBR. In this case, the mixture is made with 80 wt % SBR in order to be representative of the real proportions of the nanocomposites. The results show two separate T_g's for the mixture, identical to those of the individual polymers (−53 °C for PI-NMP and −38 °C for SBR), thus indicating the immiscibility between the two systems. This then becomes the first system in this study in which the grafted and free polymer chains are expected to have strong enough interactions to be enthalpically immiscible.

The resulting structure factors for the NP-mixed composites are reported in Figure 7 for the two samples composed of PI-NMP-SiO_2 in SBR with P/N ratios of 2.88 and 1.49, similar to that of the previous section. We observe that the PI-NMP-NP dispersion is significantly different in the SBR matrix than in the PI-Sigma matrix. The D1 sample presents a lower mean cluster size (100 nm) than the corresponding C1 (200 nm) with a larger fractal dimension larger (around 2.7), suggesting that the dispersion corresponds there more closely to the small clusters phase. More surprisingly, we can see that when reducing the P/N value, the SBR system D2 behaves opposite to the PI counterpart (C2)—the scattering intensity goes up, meaning that the mean aggregate size increases (150 nm), supplemented by the fractal dimension increase to 3, suggesting more compact aggregates.

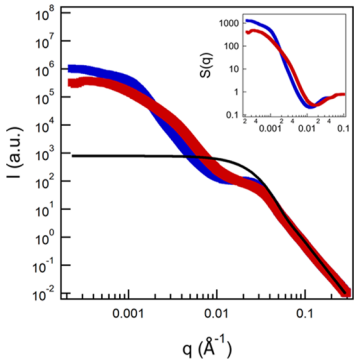

Figure 7. SAXS on PI-NMP-SiO_2 in SBR with P/N values of (red, D1) 2.88 and (blue, D2) 1.49. (Inset: Corresponding structure factors.)

These are notably more compact even than the C1 counterpart which in fact lies closer to the small cluster region on the phase diagram. While the C2 moves as expected to the connected sheet phase, the intensity goes down and the fractal dimension decreases. Such scattering behavior observed for the D2 is characteristic of phase separation which results in large, compact clusters of particles as previously observed for phase separation.[13] This is a clear impact of the enthalpic contribution that seems to dominate the entropic one seen in the microstructure mismatch, even accounting for shifts in the minor shifts in the initial state (i.e., variation over the P/N ratio) compared to the athermal and the moderated mismatched systems. As a result, the dispersion does not follow the predicted structure given by the phase diagram, but rather calls for a shift in the region boundaries to account for the enthalpic contributions.

4. CONCLUDING REMARKS

To summarize, we dispersed the PI-grafted particles in a PI matrix of constant molecular weight and showed that the dispersion follows the predicted morphology diagram of Kumar et al.[15] only in athermal conditions (i.e., the matrix and grafted polymer are identical in chemical structure) according to interactions only driven by mixing entropy. We have seen that for the matched microstructure (A), the final dispersion is in close agreement with the one given by the phase diagram. With a small change in the microstructure of the PI matrix (B,C), we observe that the entropic morphology diagram still works, except in regions near boundaries between different morphologies. This is particularly prominent with long grafted chains (B) at moderately high graft densities (the well dispersed region of the phase diagram), which seems to be more sensitive to the change in the matrix. Finally, when dispersing the grafted PI particle in a SBR matrix (D), one can see that we lose even qualitative agreement with the expected morphologies presumably because of the dominant contribution of the enthalpic interactions. We believe that these results bring new insights into the understanding of the dispersion mechanism in nanocomposites and provide a promising tool when designing controlled grafted elastomers in pursuit of specific desired macroscopic properties. Future work can explore further quantifying the enthalpic effects of the various interactions in the system that could tip the system in favor of dispersion or agglomeration (i.e., NP−NP core attraction, NP-matrix affinity, graft-matrix interaction).[32,33]

DOI: 10.1021/acs.macromol.9b01479
Macromolecules 2019, 52, 7638−7645

■ ASSOCIATED CONTENT

Supporting Information

The Supporting Information is available free of charge on the ACS Publications website at DOI: 10.1021/acs.macromol.9b01479.

PI synthesis procedure details, morphology diagram details, and SAXS structure factors (PDF)

■ AUTHOR INFORMATION

Corresponding Authors

*E-mail: sk2794@columbia.edu (S.K.K.).
*E-mail: jacques.jestin@cea.fr (J.J.).

ORCID

Andrew M. Jimenez: 0000-0001-7696-9705
Brian Benicewicz: 0000-0003-4130-1232
Sanat K. Kumar: 0000-0002-6690-2221
Didier Gigmes: 0000-0002-8833-8393
Jacques Jestin: 0000-0001-7338-7021

Author Contributions

J.J., D.G., N.M., T.P., S.K., and M.C. designed the experiments. M.B., A.M.J., and D.D. have prepared all of the samples. A.M.J. performed the TEM imaging. All of the authors have performed the experiments and participated in the analysis, interpretation, and discussion of the results. The manuscript was written through the main contribution of A.M.J., M.B., S.K., and J.J. and has been revised by all of the authors. All authors have given approval to the final version of the manuscript.

Notes

The authors declare no competing financial interest.

■ ACKNOWLEDGMENTS

We thank NYULMC DART Microscopy Lab for the assistance in EM work and ANR Nanointerprop for funding. S.K., D.D., and A.M.J. acknowledge funding from the NSF DMR-1709061.

■ REFERENCES

(1) Jayanthi, S.; Arulsankar, A.; Sundaresan, B. NanoSrTiO3-filled PEO−P(VdF-HFP)−LiClO4 electrolytes with improved electrical and thermal properties. *Appl. Phys. A* **2016**, *122*, 109.

(2) Althues, H.; Palkovits, R.; Rumplecker, A.; Simon, P.; Sigle, W.; Bredol, M.; Kynast, U.; Kaskel, S. Synthesis and characterization of transparent luminescent ZnS: Mn/PMMA nanocomposites. *Chem. Mater.* **2006**, *18*, 1068−1072.

(3) Jouault, N.; Vallat, P.; Dalmas, F.; Said, S.; Jestin, J.; Boué, F. Well-dispersed fractal aggregates as filler in polymer-silica nanocomposites: long-range effects in rheology. *Macromolecules* **2009**, *42*, 2031−2040.

(4) Attia, N. F.; Hassan, M. A.; Nour, M. A.; Geckeler, K. E. Flame-retardant materials: synergistic effect of halloysite nanotubes on the flammability properties of acrylonitrile−butadiene−styrene composites. *Polym. Int.* **2014**, *63*, 1168−1173.

(5) Liang, Y.; Cao, W.; Li, Z.; Wang, Y.; Wu, Y.; Zhang, L. Effect of octadecylamine modified graphene on thermal stability, mechanical properties and gas barrier properties of brominated butyl rubber. *Polym. Test.* **2008**, *27*, 270−276.

(6) Zhao, D.; Gimenez-Pinto, V.; Jimenez, A. M.; Zhao, L.; Jestin, J.; Kumar, S. K.; Kuei, B.; Gomez, E. D.; Prasad, A. S.; Schadler, L. S.; Khani, M. M.; Benicewicz, B. C. Tunable Multiscale Nanoparticle Ordering by Polymer Crystallization. *ACS Cent. Sci.* **2017**, *3*, 751−758.

(7) Zhao, D.; Ge, S.; Senses, E.; Akcora, P.; Jestin, J.; Kumar, S. K. Role of filler shape and connectivity on the viscoelastic behavior in polymer nanocomposites. *Macromolecules* **2015**, *48*, 5433−5438.

(8) Jouault, N.; Dalmas, F.; Boué, F.; Jestin, J. Nanoparticles reorganizations in polymer nanocomposites under large deformation. *Polymer* **2014**, *55*, 2523−2534.

(9) Robbes, A.-S.; Cousin, F.; Meneau, F.; Dalmas, F.; Boué, F.; Jestin, J. Nanocomposite Materials with Controlled Anisotropic Reinforcement Triggered by Magnetic Self-Assembly. *Macromolecules* **2011**, *44*, 8858−8865.

(10) Strawhecker, K. E.; Manias, E. Structure and Properties of Poly(vinyl alcohol)/Na+ Montmorillonite Nanocomposites. *Chem. Mater.* **2000**, *12*, 2943−2949.

(11) Schaefer, D. W.; Justice, R. S. How Nano Are Nanocomposites? *Macromolecules* **2007**, *40*, 8501−8517.

(12) Mishra, S.; Shimpi, N. G. Effect of the variation in the weight percentage of the loading and the reduction in the nanosizes of CaSO4 on the mechanical and thermal properties of styrene−butadiene rubber. *J. Appl. Polym. Sci.* **2007**, *104*, 2018−2026.

(13) Chevigny, C.; Dalmas, F.; Di Cola, E.; Gigmes, D.; Bertin, D.; Boué, F.; Jestin, J. Polymer-Grafted-Nanoparticles Nanocomposites: Dispersion, Grafted Chain Conformation, and Rheological Behavior. *Macromolecules* **2011**, *44*, 122−133.

(14) Robbes, A.-S.; Cousin, F.; Meneau, F.; Dalmas, F.; Schweins, R.; Gigmes, D.; Jestin, J. Polymer-Grafted Magnetic Nanoparticles in Nanocomposites: Curvature Effects, Conformation of Grafted Chain, and Bimodal Nanotriggering of Filler Organization by Combination of Chain Grafting and Magnetic Field. *Macromolecules* **2012**, *45*, 9220−9231.

(15) Kumar, S. K.; Jouault, N.; Benicewicz, B.; Neely, T. Nanocomposites with Polymer Grafted Nanoparticles. *Macromolecules* **2013**, *46*, 3199−3214.

(16) Heinrich, G.; Klüppel, M.; Vilgis, T. A. Reinforcement of Elastomers. *Curr. Opin. Solid State Mater. Sci.* **2002**, *6*, 195−203.

(17) Utara, S.; Jantachum, P.; Sukkaneewat, B. Effect of surface modification of silicon carbide nanoparticles on the properties of nanocomposites based on epoxidized natural rubber/natural rubber blends. *J. Appl. Polym. Sci.* **2017**, *134*, 45289.

(18) Nazhat, S. N.; Parker, S.; Riggs, P. D.; Braden, M. Blends of Isoprene-styrene/methacrylate monomer mixtures as potential soft lining material. *Biomaterials* **2001**, *22*, 2087−2093.

(19) Nazhat, S. N.; Parker, S.; Patel, M. P.; Braden, M. Isoprene-styrene copolymer elastomer and tetrahydrofurfuryl methacrylate mixtures for soft prosthetic applications. *Biomaterials* **2001**, *22*, 2411−2416.

(20) Sandusky, D.; McInnis, E. Alloy Blends of Polyurethane and Rubber. U.S. patent 20040186213 A1, March 2004.

(21) Almeida, A. P. P.; Oliveira, A. P. L. R. d.; Erbetta, C. D. Á. C.; Sousa, R. G. d.; Freitas, R. F. d. S.; Silva, M. E. S. R. e. Rheological Study of Polymers Used as Viscosity Index Improvers for Automotive Lubricant Oils. *J. Mod. Phys.* **2014**, *05*, 1085−1093.

(22) Dibbanti, M. K.; Mauri, M.; Mauri, L.; Medaglia, G.; Simonutti, R. Probing small network differences in sulfur-cured rubber compounds by combining nuclear magnetic resonance and swelling methods. *J. Appl. Polym. Sci.* **2015**, *132*, (42700) DOI: 10.1002/app.42700.

(23) Mary, C.; Philippon, D.; Lafarge, L.; Laurent, D.; Rondelez, F.; Bair, S.; Vergne, P. New Insight into the Relationship Between Molecular Effects and the Rheological Behavior of Polymer-Thickened Lubricants Under High Pressure. *Tribol. Lett.* **2013**, *52*, 357−369.

(24) Fröhlich, J.; Niedermeier, W.; Luginsland, H.-D. The effect of filler−filler and filler−elastomer interaction on rubber reinforcement. *Compos. Appl. Sci. Manuf.* **2005**, *36*, 449−460.

(25) Bouty, A.; Petitjean, L.; Degrandcourt, C.; Gummel, J.; Kwaśniewski, P.; Meneau, F.; Boué, F.; Couty, M.; Jestin, J. Nanofiller Structure and Reinforcement in Model Silica/Rubber Composites: A Quantitative Correlation Driven by Interfacial Agents. *Macromolecules* **2014**, *47*, 5365−5378.

DOI: 10.1021/acs.macromol.9b01479
Macromolecules 2019, 52, 7638−7645

(26) Bouty, A.; Petitjean, L.; Chatard, J.; Matmour, R.; Degrandcourt, C.; Schweins, R.; Meneau, F.; Couty, M.; Jestin, J. Interplay between polymer chain conformation and nanoparticle assembly in model industrial silica/rubber nanocomposites. *Faraday Discuss.* **2016**, *186*, 805−325−343.
(27) Baeza, G. P.; Genix, A.-C.; Degrandcourt, C.; Petitjean, L.; Gummel, J.; Couty, M.; Oberdisse, J. Multiscale Filler Structure in Simplified Industrial Nanocomposite Silica/SBR Systems Studied by SAXS and TEM. *Macromolecules* **2013**, *46*, 317−329.
(28) Hosseini, S. M.; Torbati-Fard, N.; Kiyani, H.; Razzaghi-Kashani, M. Comparative role of Interface in reinforcing mechanisms of Nano silica modified by Silanes and liquid rubber in SBR composites. *J. Polym. Res.* **2016**, *23*, (203) DOI: 10.1007/s10965-016-1096-0.
(29) Khani, M. M.; Abbas, Z. M.; Benicewicz, B. C. Well-Defined Polyisoprene-Grafted Silica Nanoparticles via the RAFT Process. *J. Polym. Sci., Part A: Polym. Chem.* **2017**, *55*, 1493−1501.
(30) Bonnevide, M.; Phan, T. N. T.; Malicki, N.; Kumar, S. K.; Couty, C.; Gigmes, D.; Jestin, J. Synthesis of Polyisoprene, Polybutadiene and Styrene Butadiene Rubber Grafted Silica Nanoparticles by Nitroxide-Mediated Polymerization, *Polymer Journal* **2019**, to be submitted.
(31) Akcora, P.; Liu, H.; Kumar, S. K.; Moll, J.; Li, Y.; Benicewicz, B. C.; Schadler, L. S.; Acehan, D.; Panagiotopoulos, A. Z.; Pryamitsyn, V.; Ganesan, V.; Ilavsky, J.; Thiyagarajan, P.; Colby, R. H.; Douglas, J. F. Anisotropic self-assembly of spherical polymer-grafted nanoparticles. *Nat. Mater.* **2009**, *8*, 354−359.
(32) Martin, T. B.; Mongcopa, K. I. S.; Ashkar, R.; Butler, P.; Krishnamoorti, R.; Jayaraman, A. Wetting−Dewetting and Dispersion−Aggregation Transitions Are Distinct for Polymer Grafted Nanoparticles in Chemically Dissimilar Polymer Matrix. *J. Am. Chem. Soc.* **2015**, *137*, 10624−10631.
(33) Zhang, R.; Lee, B.; Bockstaller, M. R.; Kumar, S. K.; Stafford, C. M.; Douglas, J. F.; Raghavan, D.; Karim, A. Pattern-Directed Phase Separation of Polymer-Grafted Nanoparticles in a Homopolymer Matrix. *Macromolecules* **2016**, *49*, 3965−3974.

DOI: 10.1021/acs.macromol.9b01479
Macromolecules 2019, 52, 7638−7645